Clays and Clay Minerals, Vol. 50, No. 4, 514–524, 2002.

KEROLITE IN CARBONATE-RICH SPELEOTHEMS AND MICROBIAL DEPOSITS FROM BASALTIC CAVES, KAUAI, HAWAII

RICHARD J. LÉVEILLÉ*, FRED J. LONGSTAFFE AND WILLIAM S. FYFE

Department of Earth Sciences, The University of Western Ontario, London, Ontario, Canada N6A 5B7

Abstract—The occurrence of kerolite in association with various secondary Ca-Mg carbonate mineral deposits (speleothems) was identified in basaltic sea caves on the island of Kauai, Hawaii. Kerolite is the dominant clay mineral in the deposits. X-ray diffraction (XRD) peaks of the kerolite are characteristically broadened indicating its extremely poor crystallinity. Few changes were observed in the XRD patterns of this kerolite when it was subjected to various humidity, temperature and ethylene-glycol treatments. The crystals appear as flaky masses with irregular or jagged edges in scanning (SEM) and transmission electron microscopy (TEM). Electron probe and energy dispersive X-ray (EDX) microanalysis show that the clay material is dominated by Mg-Si-O, with minor amounts of Al and Ca in some samples. The chemical composition, thermal analysis and TEM observations suggest that smaller amounts of an amorphous serpentine-like phase are mixed with the kerolite. Kerolite is often the only mineral associated with poorly mineralized, actively-growing microbial mats in these caves and it is common in completely lithified microbial mats. The latter commonly have microstromatolitic structures with kerolite as a dominant phase. These features suggest that kerolite formation is at least in part a result of microbial activity. The abundant extracellular polymers of the mat-forming bacteria bind and concentrate ions (Mg^{2+}, silica) from solution and serve as nucleation sites for kerolite precipitation. Conditions within the mats also probably lead to formation of Mg-Si-gels, amorphous Mg-silicate precursors and ultimately kerolite. Evaporation of the cave solutions may also contribute to kerolite formation.

Key Words—Bacteria, Basalt, Caves, Clay, Hawaii, Kauai, Kerolite, Magnesium, Microbial Mats, Speleothems.

INTRODUCTION

This paper describes kerolite and associated clay minerals from Kauai sea caves, using powder XRD, electron microscopy, electron probe microanalysis and thermal analysis. To the best of our knowledge, this is the first description of kerolite in Hawaii, as well as in basaltic caves. This is also believed to be the first known association of kerolite with bacteria and microbial mats.

Authigenesis of clay minerals in caves is a widespread process, though it has received relatively little attention compared to carbonate minerals (Hill and Forti, 1997). Finlayson and Webb (1988) described poorly-ordered sepiolite and halloysite interbedded with calcite in secondary mineral deposits (speleothems) from granitic caves of the Peninsular Ranges and Sierra Nevada batholiths, California. White (1976) mentioned the presence of authigenic 'endellite' (1 nm halloysite) in soils from Carlsbad Caverns and sepiolite on the ends of speleothems in the Zbrazor Caves in the former Czechoslovakia. Polyak and Güven (2000) described Mg-clays (including a minor amount of a poorly crystalline, Mg-rich kerolite-like mineral) occurring in carbonate- and smectite-rich speleothems from dolomite-hosted caves in the Guadalupe Mountains, New Mexico. Carbonates and clays have also been found together in various basaltic caves, but little mineralogical work has been performed on these occurrences (*e.g.* Waters *et al.*, 1990; Kashima, 1993; Sarkar *et al.*, 1998).

Kerolite ($Mg_3Si_4O_{10}(OH)_2 \cdot nH_2O$) is a relatively uncommon, hydrated and highly disordered variety of talc (Maksimović, 1966; Brindley *et al.*, 1977; Brindley and Brown, 1980). Its basal XRD reflections are typically broadened compared to those of talc, indicating a small crystal size and extreme disorder (Brindley *et al.*, 1977). Kerolite shows only an occasional poor response to ethylene glycol treatment, and only then after several days of exposure (Brindley *et al.*, 1977). These characteristics allow it to be differentiated from stevensite, a Mg-rich smectite, and from talc, which is well-ordered. However, because of its d_{001} diffraction centered around 1.0 nm, kerolite may be misidentified as illite in sedimentary samples containing a mixture of clays and other minerals (Stoessell and Hay, 1978). Kerolite may also be mistaken for stevensite, saponite or sepiolite based on chemical composition alone.

Secondary mineral deposits in basaltic sea caves on the island of Kauai, Hawaii, were first described in detail by Léveillé *et al.* (2000a). The deposits are extremely variable in macroscopic character, ranging from extensive mm-thin, powdery coatings to hard crusts several cm thick, which commonly occur in circular patches of a few tens of cm in diameter. Complex assemblages of aragonite, calcite, monohydrocalcite, dolomite, magnesite, hydromagnesite and a 1.0 nm Mg-clay, identified as kerolite, were recognized by XRD and electron probe

* E-mail address of corresponding author:
c1730@er.uqam.ca

microanalysis. Minor amounts of gypsum occur almost exclusively in magnesite-rich, thin coatings.

The association of these cave deposits with actively-forming microbial mats was demonstrated by Léveillé *et al.* (2000b). Scanning and transmission electron microscopy revealed that the mats are dominated by bacteria and cyanobacteria, and contain abundant extracellular polymeric substances (EPS) forming a dense, hydrated mucus. The mats vary in their degree of mineralization; some show no mineralization, whereas others are extensively mineralized. Microstromatolitic structures, consisting of alternating Mg-clay- and aragonite/calcite-rich layers, are common in the thicker mineral deposits and suggest that they are the lithified remains of microbial mats (Léveillé *et al.*, 2000b). In addition to being found in these structures, kerolite also typically appears in poorly mineralized microbial mats and as powdery masses. No clay was found in the thin, powdery coatings dominated by magnesite or in carbonate-filled vesicles near the basalt surface (Léveillé *et al.*, 2000a).

Isotopic and geochemical evidence indicate that the secondary minerals have crystallized from Ca-Mg-Si-HCO_3-dominated fresh water (pH ~8) seeping from the basaltic host rock, and this mineralization process is ongoing at some locations (Léveillé, 2000). The cave and surface waters were found to be, for the most part, close to saturation with respect to kerolite (Léveillé, 2000). Modeling of the changes in concentration of the cave-water solutes as a result of evaporation showed that kerolite could become supersaturated upon equilibration of the water with the cave atmosphere ($P_{CO_2} = 10^{-3.5}$), or upon minor evaporative concentration of solutes and a corresponding small increase in pH (Léveillé, 2000).

MATERIALS AND METHODS

Seven speleothem samples collected from two of the large 'wet' and 'dry' caves on the north coast of Kauai, Hawaii (see Léveillé *et al.*, 2000a, b) were crushed to < ~2 mm grain-size and placed in a sodium acetate buffered acetic acid solution (pH ~5.0–5.2) for several days at ~35–65°C to selectively dissolve the carbonates (Ostrom, 1961). After washing in distilled water by centrifugation, drying in an oven at 65°C and grinding to < ~0.6 mm, the samples were dispersed using an ultrasonic agitator. The <2 μm fraction was then separated by settling in 30 cm high glass columns. Bleach (6%) was added to the separated material as a flocculant and to oxidize organic matter. The separated material was then washed in distilled water several times by centrifugation.

Randomly-oriented specimens of the separated <2 μm material were prepared for XRD analysis using glass mounts. Ca and K saturations of other portions of the <2 μm fraction were prepared using 2 M $CaCl_2$ and 2 M KCl, respectively. Following thorough washing and freeze drying, ceramic disk mounts of the Ca- and K-saturated material (~20 mg each) were prepared to obtain preferred-oriented samples for XRD analysis. In preparation of these mounts, some samples did not completely disperse after ultrasonication (even after 2–3 min) and after drying, many mounts showed desiccation cracks. After trial and error, and following the suggestions of Hay *et al.* (1995), the following steps were found to be the most effective for sample preparation. Samples were first gently ground and placed in water overnight. Then, the samples were wet-ground in a ball-mill for ~1 min. Finally, the samples were dispersed by ultrasonication before preparing the disk mounts.

Powder XRD analysis was performed using a Rigaku diffractometer, equipped with a rotating anode (CoKα source; 160 mA and 45 kV) and a graphite monochromator. Scans of randomly-oriented samples were performed at a rate of 10°2θ/min and a step size of 0.02°2θ, while those for oriented samples were performed at a rate of 2°2θ/min with the same step size. The K-saturated, oriented specimens were analyzed at 54% relative humidity (RH) and at 0% RH. They were also analyzed after heating to 300 and 550°C. The Ca-saturated, oriented specimens were first analyzed at 54% RH. They were then exposed to an ethylene glycol atmosphere for extended periods (>4 weeks) and then analyzed again.

Polished thin-sections cut from resin-impregnated speleothem samples, or rocks with speleothem coatings, were examined petrographically. Four of these sections were then carbon-coated and examined again using a JEOL JXA 8600 electron probe. Typically, 9 or 10 spot analyses were performed in clay-rich areas on a given thin-section to determine clay composition. Quantitative compositional data were obtained using wavelength dispersive X-ray spectroscopy and appropriate standards.

Three sub-samples of the <2 μm material were examined by transmission electron microscopy (TEM), using a Philips CM10 TEM at an accelerating voltage of 80 kV. Samples were dispersed in micropore-filtered distilled water by ultrasonication for 1–2 min and pipetted onto carbon-coated nickel grids with Formvar coatings. Two of these samples were also analyzed by energy dispersive X-ray spectroscopy (EDS) at an accelerating voltage of 100 kV using a Philips EM400T TEM equipped with a Link LZ-5 EDS system. Samples of microbial mats were also examined as described in Léveillé *et al.* (2000b) using a JEOL JEM-2000 FX TEM equipped with a PGT Prism EDS system.

Freshly exposed surfaces of two bulk kerolite-rich samples were analyzed by scanning electron microscopy (SEM), using a Hitachi S-4500 Field Emission SEM equipped with an EDAX X-ray analysis system. The SEM was operated at an accelerating voltage of 15 kV with a working distance of 15 mm as a suitable compromise between minimizing charging and sample

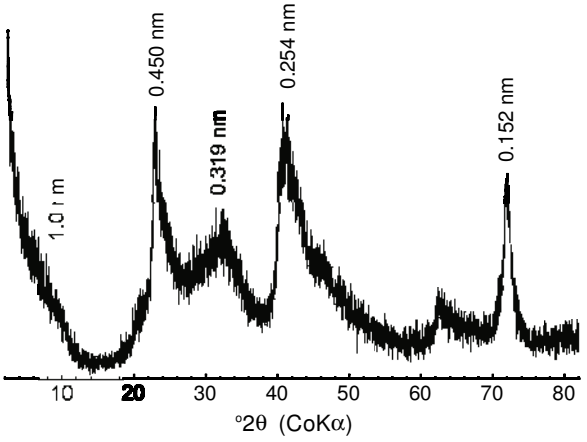

Figure 1. XRD pattern of a randomly-oriented, bulk (untreated) speleothem sample consisting mainly of poorly-ordered kerolite. Major *d*-spacings are labeled.

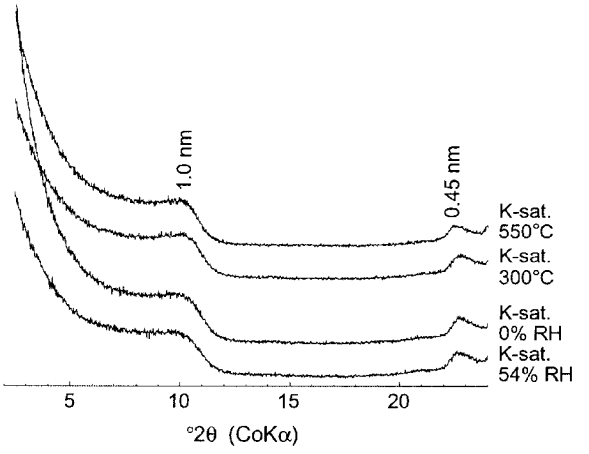

Figure 2. Representative XRD patterns of oriented mounts of a K-saturated, <2 μm kerolite sample at different relative humidities (RH) and temperatures.

damage, and obtaining sufficient counts during EDS analysis.

Differential thermal analysis (DTA) and thermogravimetric (TG) measurements were performed using a Linseis L81 Thermobalance. Approximately 15–20 mg of the <2 μm clay fraction was heated from ~20 to 105°C at 1°C/min and from ~105 to 1000°C at 10°C/min, along with alumina as a standard. In some cases, the sample was analyzed by XRD after heating to 1000°C to determine if temperature-induced mineralogical transformations had occurred.

RESULTS

X-ray diffraction

All samples examined by XRD showed similar patterns with poor peak sharpness and a broad, asymmetric peak at ~1.0 nm (Figure 1), which corresponds to the d_{001} peak of kerolite (Brindley *et al.*, 1977). There were minor differences between the samples but all seven showed broad diffractions at ~0.45, 0.32, 0.25 and 0.152 nm, the latter representing the d_{060} spacing, indicating a trioctahedral structure. The peaks at ~0.45 and ~0.25 nm are distinctively asymmetric and steeper towards lower angles of 2θ. Such asymmetry was reported previously for kerolite (*cf.* Brindley *et al.*, 1977; Pozo and Casas, 1999).

Samples prepared to enhance the orientation of 00*l* reflections (preferred orientation) did not have XRD patterns (Figures 2,3) that were significantly different from those of the randomly-oriented specimens. The K-saturated and Ca-saturated samples were nearly identical for similar treatments. All of the broad peaks remained in the K-saturated samples after treatment at 550°C, although a slight sharpening of the d_{001} reflection was observed after heating to 300°C and 550°C (Figure 2). A bulk sample heated to 500°C during DTA/TG analysis showed no obvious differences in its XRD pattern from the unheated bulk sample, except for a slightly more defined d_{001} reflection at ~1.0 nm. Variations in XRD patterns as a consequence of treatments at different relative humidities were negligible (*e.g.* K-saturated at 54% RH *vs.* K-saturated at 0% RH; Figure 2). Ethylene glycol treatment for more than 4 weeks led to only minor changes in the intensity of the 1.0 and 0.45 nm reflections relative to the same Ca-saturated sample analyzed at 54% RH (Figure 3). The main change resulting from glycolation was a slightly improved resolution of the 1.0 nm reflection towards lower angles, and decreased resolution of the 0.45 nm reflection towards higher angles. Reflections associated with smectite or smectite interlayers were not observed in any ethylene glycol-treated sample. The d_{001} diffraction

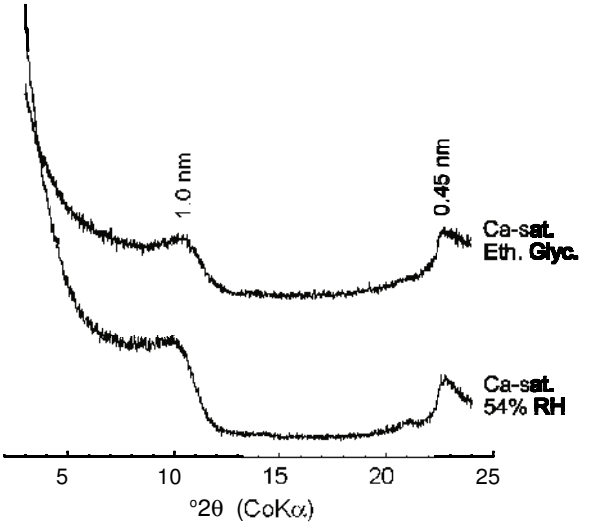

Figure 3. Representative XRD patterns of oriented mounts of a Ca-saturated, <2 μm kerolite sample. The upper trace represents a sample solvated in an ethylene glycol-saturated atmosphere for >4 weeks.

https://doi.org/10.1346/000986002320514235 Published online by Cambridge University Press

of smectites such as stevensite (or kerolite-stevensite) tend to collapse to ~1.0 nm upon heating to temperatures >375–400°C (Hay *et al.*, 1995; Elton *et al.*, 1997); such behavior was not observed in the Kauai material. Similarly, no diffractions were evident at 0.7 or 1.2 nm for any of the samples, indicating that neither crystalline serpentine nor sepiolite are abundant in these samples. No other silicates were identified by XRD.

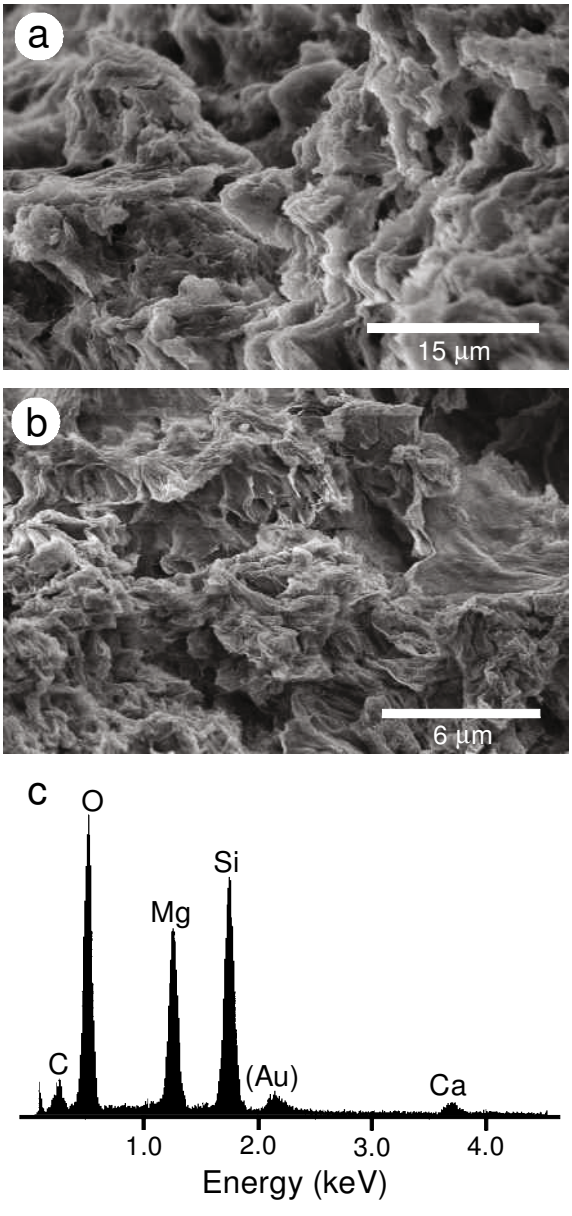

Figure 4. SEM images of irregularly-shaped, stacked flakes (a) and wavy, irregular masses (b) of kerolite-rich material from Kauai cave deposits. (c) EDS spectrum from kerolite-rich material seen in part a, showing the dominance of Mg, Si and O. Ca and C are probably from Ca carbonate. Au is from the gold coating.

Petrography and electron microscopy

The kerolite appears as dark-brown, reddish-brown or dark-gray masses under the petrographic microscope. Its extremely fine grain-size precluded any detailed observations of its crystallinity using this method.

In SEM, the kerolite generally has an irregular appearance and a flaky, wavy texture; it typically occurs as irregular stacked plates (Figure 4a,b). Qualitative analysis by EDS confirmed that the kerolite is composed almost entirely of Mg, Si and O (Figure 4c). Small amounts of Ca, C and Al were detected within the masses of kerolite in some samples. Desiccation or shrinkage cracks <10 µm in width are common in many samples. Stoessell (1988) described similar-looking, though extremely fine-grained, massive kerolite as crinkly and flaky or smectitic looking in SEM. The Kauai samples are also similar in appearance to the mixed-layer kerolite-stevensite examined by Hay *et al.* (1995; their Figure 6) and described as a boxwork of wavy sheets.

Although clumping and aggregation were often problems in the samples analyzed by TEM, individual particles were common enough to allow inspection of particle shape and size. The kerolite crystals are typically sub-rounded in outline with irregular, jagged or fluffy edges, which often curl upon themselves (Figure 5a,b). Aggregates of many plates are common, and can be ~3–4 µm in diameter. Individual crystals are typically ~1 µm in diameter. Qualitative EDS analysis showed that Mg, Si and O are the only major constituents (Figure 5c). Minor amounts of Al were detected in some samples. In both the <2 µm isolates and the bulk material, non-distinct, material amorphous to X-rays is also commonly observed. The Kauai kerolite is similar in appearance to that studied by Maksimović (1966), who described it as ...irregular fluffy masses with ill-defined edges.... In some cases, it resembles the packed hollow sphere texture found in the Tagus Basin pink clays composed of poorly crystalline stevensite, saponite and talc (Santiago Buey *et al.*, 2000).

Small amounts of a euhedral, platy mineral with a hexagonal shape, ~1–2 µm in size were also observed by TEM (Figure 5b). Analysis by EDS revealed it to be composed predominantly of Al, Si and O (Figure 5d). This phase is probably kaolinite. Smaller pseudo-hexagonal plates and pseudo-rectangular tablets (<500 nm) are also present in trace quantities (Figure 6a). Both show well-developed crystal boundaries and they occur individually and in stacks. These may also be kaolinite. However, no other evidence for kaolinite was found in the bulk XRD analyses or in electron probe microanalyses (EPM), except for the small amount of Al detected in some of the kerolite-rich masses. Traces of extremely small (<250 nm in length) needle-like crystals are also present in these samples (Figure 6b). No useful compositional information was obtained for the crystals illustrated in Figure 6.

https://doi.org/10.1346/000986002320514235 Published online by Cambridge University Press

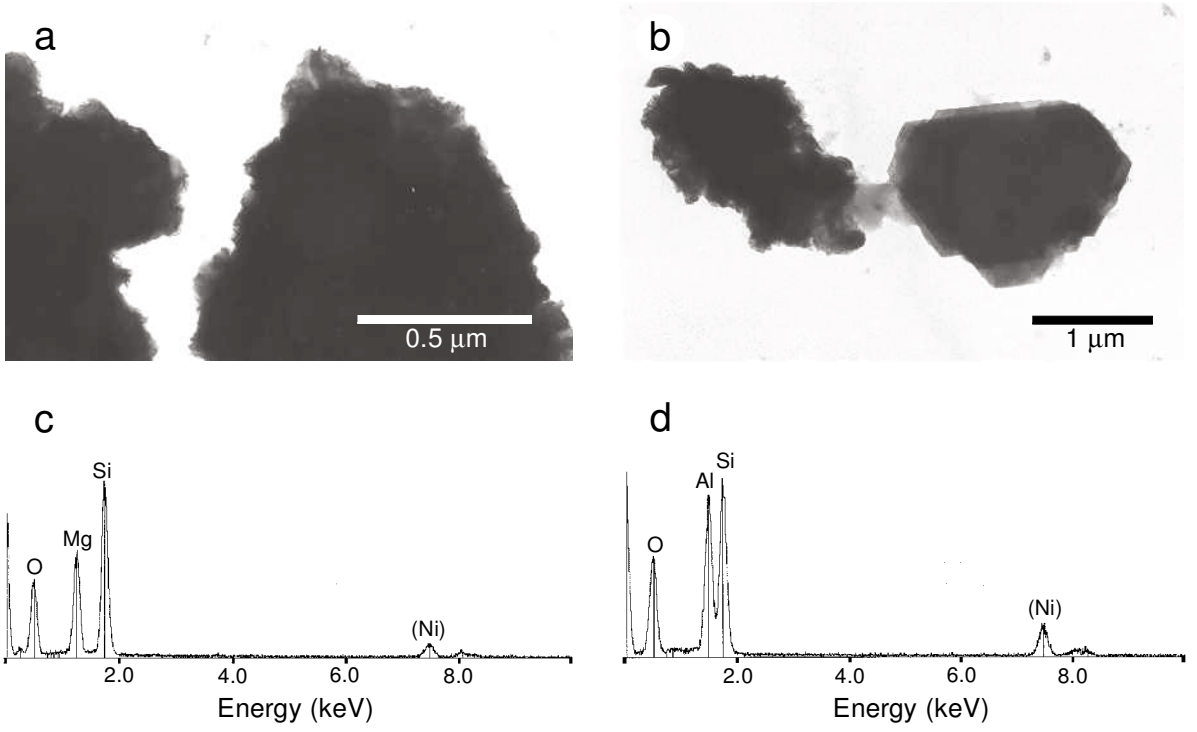

Figure 5. (a) TEM image of irregularly-shaped kerolite grains, with ragged edges. These crystals have the sharpest XRD peaks of all the kerolite examined in this study. (b) TEM photomicrograph of kerolite (left) and an Al-rich, hexagonal mineral (right) believed to be kaolinite. (c) EDS spectrum of kerolite showing Mg, Si and O as the only constituents. (d) EDS spectrum of putative kaolinite, showing Al, Si and O. Ni is from the Ni grids.

Poorly mineralized microbial mat material analyzed by TEM-EDS consistently showed abundant Mg and Si concentrated within dense EPS surrounding bacterial cells (Figure 7). This is consistent with the previous findings of Léveillé *et al.* (2000b).

Chemical composition

Major oxide compositions of the Kauai kerolite, as determined by EPM, are summarized in Table 1. No cations other than Mg and Si are present in significant amounts. In two separate spot analyses, the Al_2O_3 content was found to be ~2%, though it is typically <<1%. All other oxide contents are <1%. In all four samples, the structural formula calculations show that there is a deficiency of SiO_2 (<4 tetrahedral cations) and an excess of MgO (>3 octahedral cations), assuming a unit-cell with $O_{10}(OH)_2$ and a charge balance of 22 for kerolite. The SiO_2/MgO molar ratios for the kerolite range between 1.06 and 1.27 (Table 1); they are all below the expected theoretical value of 1.33 for 'ideal' kerolite.

The two samples from the Wet Cave (WC-05 and WC-09) are similar in chemical composition to previously reported results for kerolite or kerolite-stevensite, whereas those of the two Dry Cave samples (DC-06 and DC-07) trend towards the composition of kerolite-rich deweylite (Figure 8; see below). These differences may be related to the compositions of the cave waters; the Dry Cave waters have a Si/Mg ratio of ~1.3, whereas that in the Wet Cave waters is ~2.5 (Léveillé, 2000). However, EPM does not permit accurate monomineralic analyses to be obtained from the fine-grained clay component. Hence, the results reported in Table 1 may include quantities of phases like serpentine, which can be physically mixed or mineralogically interstratified with the massive kerolite. Any significant serpentine impurity in a kerolite-rich sample would result in octahedral cation (Mg) contents in excess of 3 and tetrahedral cation (Si) contents of <4 for the kerolite.

Thermal behavior

The results of the thermal analysis are presented in Figure 9. Typically, DTA traces for the kerolite-rich samples show two moderately sharp endothermic peaks; one at ~100°C, and another at ~810°C. A broad exothermic peak at 300–350°C and a very sharp exothermic peak at ~820–825°C are also present. The two endothermic peaks are slightly less well defined in samples judged to be less crystalline based on their XRD patterns. The TGA curves indicate that ~5–6.5% of the weight is lost rapidly up to ~110–120°C, followed by a gradual weight loss of 5–9% to ~780°C, with a final rapid loss of ~2–2.5% between 780 and 820°C (total weight loss = ~13–18%). Samples heated to 1000°C and

https://doi.org/10.1346/000986002320514235 Published online by Cambridge University Press

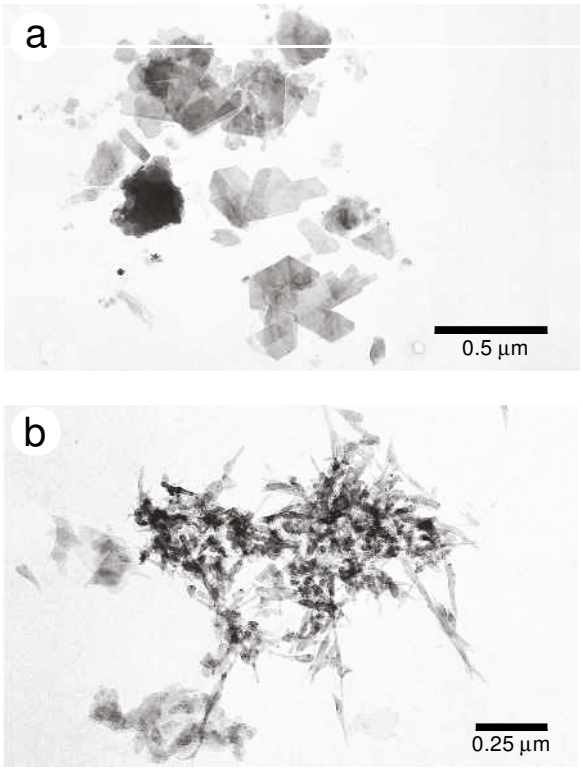

Figure 6. (a) TEM image of uncommon, pseudo-hexagonal, fine-grained crystals, possibly of kaolinite. (b) TEM image of extremely fine, needle-like crystals, possibly of serpentine, found in trace amounts. No compositional information was obtained for these minerals.

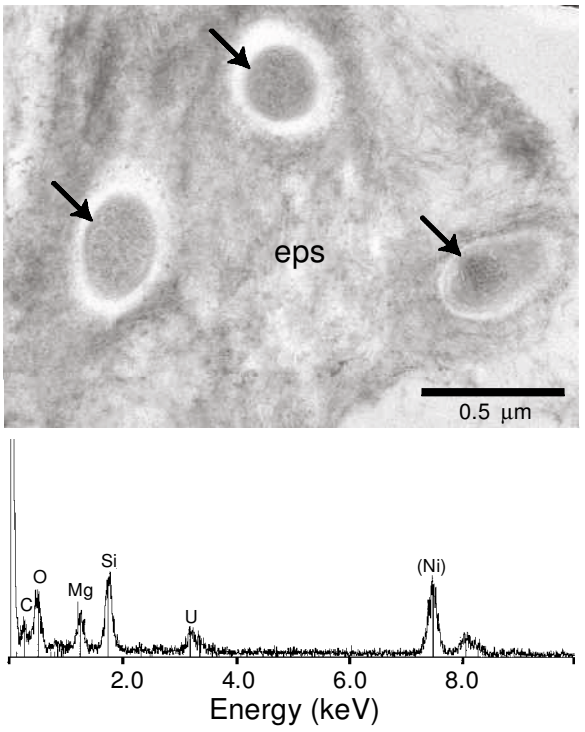

Figure 7. TEM image of a microbial mat material from the Kauai caves. Three bacterial cells (arrows) are completely surrounded by a dense matrix of fibrillar extracellular polymeric substances (eps). The eps contains abundant Mg, Si, O and C as revealed by EDS analysis. U is from uranyl acetate stain added to increase contrast. Ni is from the Ni grid.

above were subsequently analyzed by XRD; they showed no kerolite diffraction peaks, but instead displayed reflections that correspond to forsterite and enstatite.

The DTA/TG results are generally consistent with previous findings for kerolite and similar material. The two endothermic peaks at ~100°C and ~810°C are characteristic of kerolite and they probably correspond to the loss of adsorbed water and dehydroxylation (collapse) of the structure, respectively (*e.g.* Maksimović, 1966; Brindley *et al.*, 1977). An exothermic peak at ~830°C immediately following an endothermic peak (such as that seen in Figure 9) is generally diagnostic of the breakdown (dehydroxylation) and recrystallization of serpentine to forsterite, or sepiolite to enstatite (Mackenzie, 1970; Morandi and Poppi, 1974). The broad exothermic peak at ~300–350°C (Figure 9) may also be attributed in part to serpentine (Maksimović, 1966; Mackenzie, 1970; Morandi and Poppi, 1974) or to the oxidation of organic matter (Mackenzie, 1970). Although bleach was added to the material during the clay separation process, some organic matter may not have been completely oxidized. However, the DTA/TG patterns for the Kauai samples closely resemble those of Morandi and Poppi (1974) for chrysotile-rich deweylites.

DISCUSSION

Nature of the Kauai kerolite and associated clay minerals

Our XRD findings are consistent with kerolite being the dominant phase in the <2 μm material and the dominant clay mineral in the cave deposits. The broadening of kerolite's basal reflections is generally ascribed to poor ordering (disordered layer stacking) and (or) small crystallite size (Brindley *et al.*, 1977; Brindley and Brown, 1980). However, the reflections for the Kauai kerolite are even broader than reported in most previous analyses. Because the Kauai kerolite crystals appear to be relatively large (*i.e.* ~1 μm), as revealed by TEM, the broadening of its basal reflections is probably a result of its extreme disorder. The difficulties encountered during the preparation of ceramic disk mounts of preferred-oriented material were probably a consequence of this extreme disorder. Hay *et al.* (1986) also noted that kerolite was more difficult to disperse in water than Mg-smectite from the same localities. Similarly, Martin de Vidales *et al.* (1991) found it physically impossible to obtain completely oriented samples of kerolite-rich material on glass slides after drying, despite using a dispersant and varying the proportions of solid to liquid

https://doi.org/10.1346/000986002320514235 Published online by Cambridge University Press

Table 1. Chemical analyses[1] and structural formulae[2] of Kauai kerolite.

	WC-05	WC-09	DC-06	DC-07
SiO_2	54.41	57.09	53.27	54.24
Al_2O_3	0.37	0.26	0.13	0.19
FeO	0.10	0.03	0.02	0.04
MnO	0.01	<0.01	0.03	0.01
MgO	28.79	31.89	33.62	32.08
CaO	0.25	0.36	0.13	0.22
Na_2O	0.31	0.29	0.52	0.38
K_2O	0.09	0.17	0.15	0.14
H_2O_{tot}[3]	14	n.a.	18	n.a.
Total	98.33	n.a.	105.87	n.a.
Si	3.909	3.853	3.716	3.791
Al	0.031	0.021	0.011	0.016
ΣTetr.	3.94	3.87	3.73	3.81
Fe	0.006	0.002	0.001	0.002
Mn	0.001	0.001	0.002	0.001
Mg	3.083	3.208	3.497	3.343
ΣOct.	3.09	3.21	3.50	3.35
Si/Mg	1.27	1.20	1.06	1.13
Ca	0.019	0.026	0.010	0.016
Na	0.043	0.038	0.070	0.052
K	0.008	0.015	0.013	0.012

[1] Chemical analyses are averages of 9–10 EPM spot analyses per sample.
[2] Structural formulae based on $O_{10}(OH)_2$ and a charge balance of 22.
[3] Water data from thermogravimetric analysis (see text for details).

in suspension, or the time of ultrasonic treatment. The extreme disorder of the Kauai kerolite may be a consequence of bacterially-mediated crystallization (see below) as bacterial neoformation of clay-like minerals typically produces poorly-ordered crystals or amorphous phases (Tazaki, 1997; Konhauser and Urrutia, 1999).

Together, the bulk chemical compositions and the DTA/TG results may suggest that a serpentine-like phase coexists with the kerolite. This phase is probably amorphous or extremely disordered and extremely fine-grained as no diagnostic 0.7 nm peak was apparent in the XRD patterns. The fine (<250 nm) needle-like crystals observed in TEM, but not identified, may be serpentine. Kerolite has previously been found mixed with poorly-crystalline serpentine, both in natural settings and in experimental reaction products (*e.g.* Brindley *et al.*, 1977; Sakamoto *et al.*, 1981; Gíslason *et al.*, 1993). The term 'deweylite' has been used to describe intimate mixtures of an extremely fine-grained, highly-disordered, talc-like mineral (*i.e.* kerolite-like) and a disordered serpentine mineral, typically chrysotile, in varying proportions (Bish and Brindley, 1978). Deweylites typically have chemical compositions intermediate to 1:1 and 2:1 type Mg-clays (Figure 8) and have distinct XRD patterns with major peaks at both 1.0 and 0.7 nm, corresponding to kerolite and serpentine, respectively (Speakman and Majumdar, 1971; Bish and Brindley, 1978; Brindley and Brown, 1980). However, serpentine may not be recognized by XRD in kerolite-rich materials, even when it makes up as much as 20% of the sample (Brindley and Brown, 1980). In the case of the Kauai samples, simple mixing calculations based on the MgO% composition of ideal serpentine and the average of published kerolite compositions indicate that ~12–26% of serpentine-like material could be present with the kerolite. However, because of the lack of 0.7 nm reflections for the present samples, the presence of crystalline serpentine cannot be confirmed and the material should therefore not be referred to as deweylite.

It is also possible that the Kauai kerolite, which appears to be more highly disordered than previously-reported occurrences, behaves somewhat like serpentine when heated, and re-crystallizes to form forsterite and enstatite. This could explain the large exothermic DTA peak at ~830°C, which appears to be rather large for the putative amount of serpentine present in these samples. In general, trioctahedral minerals re-crystallize immediately after dehydroxylation (Mackenzie, 1970). This is even more likely for poorly-ordered minerals with simple chemical compositions, such as the Kauai kerolite. No previous DTA studies of kerolite have reported such a heat-induced structural transformation. However, Sakamoto *et al.* (1981) did report an exothermic peak at ~820°C for poorly-crystallized material (*i.e.* stevensite, 'hydrated talc' or talc, and minor serpentine) formed from MgO-SiO_2 gels at high temperatures.

The apparent presence of an amorphous serpentine-like phase could also be an artifact of this kerolite having a chemical composition that varies widely from 'ideal kerolite', possibly because of its extreme disorder. Natural kerolite is known to deviate from its ideal chemical composition (see Figure 8). Bacterially-mediated neoformation of clay-like minerals, in particular, typically leads to phases which can differ significantly from their ideal compositions (Tazaki, 1997; Konhauser and Urrutia, 1999). In addition, the higher SiO_2/MgO ratio of the Wet Cave clay compared to that of the Dry Cave clay may be related to the chemical composition of the cave waters. This difference in initial solution composition may also have contributed to the extreme disorder of the kerolite, especially in the Dry Cave. Caillère *et al.* (1963) showed that a higher initial SiO_2/MgO in gels (*e.g.* 1.10 *vs.* 1.03) could produce more crystalline reaction products.

The inherent difficulty in recognizing and identifying kerolite in mixed mineral samples (*e.g.* soils, sediments, speleothems), its poor crystallinity and its abundance in the present deposits hint that it may have been overlooked in previous studies, both in Hawaii and elsewhere.

https://doi.org/10.1346/000986002320514235 Published online by Cambridge University Press

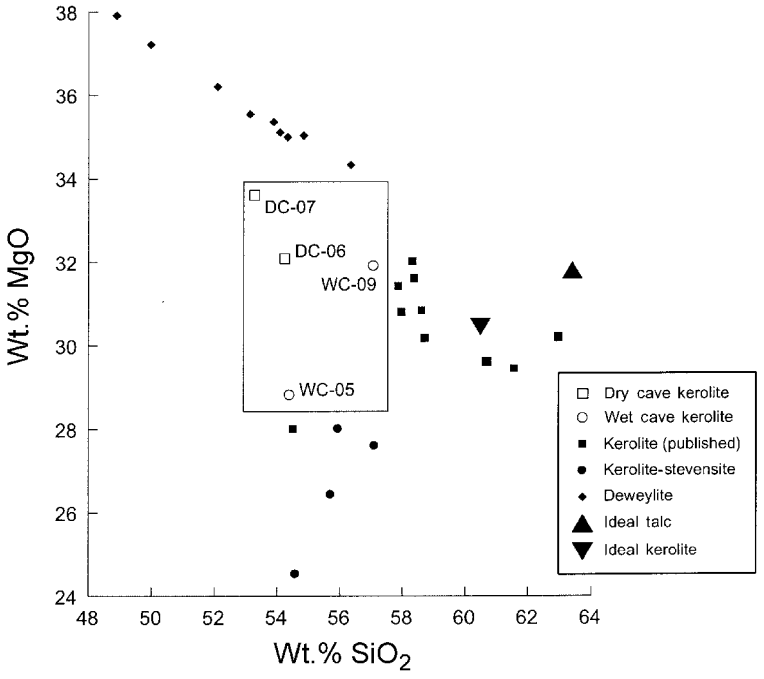

Figure 8. Plot of MgO *vs.* SiO_2 for four kerolite samples from the Kauai caves (open symbols in box) and published compositions of kerolite and associated Mg silicates from previous studies (solid squares). Oxide wt.% values of the Kauai cave kerolite are averages of several electron probe spot microanalyses (Table 1). The deweylite data are taken from Bish and Brindley (1978) and represent different ratios of kerolite to serpentine. The kerolite data are taken from Brindley *et al.* (1977), Stoessell (1988) and Elton *et al.* (1997). The data for mixed-layer kerolite-stevensite are taken from Elton *et al.* (1997) and Pozo and Casas (1999).

Formation of kerolite and related minerals

Based on thermodynamic stabilities, authigenic Mg silicates are predicted to form under certain low-temperature conditions, but they are relatively uncommon in near-surface environments (Stoessell, 1988). Talc and serpentine are the stable Mg silicates at 25°C and 1 bar in most natural waters, but they rarely form at low temperatures because of kinetic constraints (Jones, 1986; Stoessell, 1988). The presence of Al in an aqueous, Si-containing system will favor the formation of dioctahedral 1:1 clays (*e.g.* kaolinite), which are common authigenic products of silicate weathering (Caillère *et al.*, 1963; Stoessell, 1988). For the normal range of SiO_2 concentrations in natural waters at normal surface conditions (*e.g.* ~5–25 ppm; Langmuir, 1997) or in waters supersaturated with respect to quartz, kerolite is metastable with respect to sepiolite. However, the

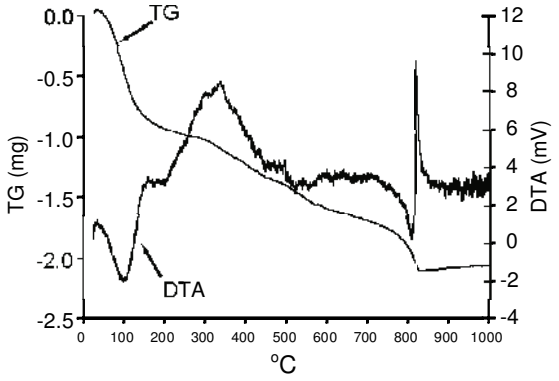

Figure 9. Differential thermal (DTA) and thermogravimetric (TG) analysis curves for kerolite-rich material from Kauai heated at a rate of 10°C/min.

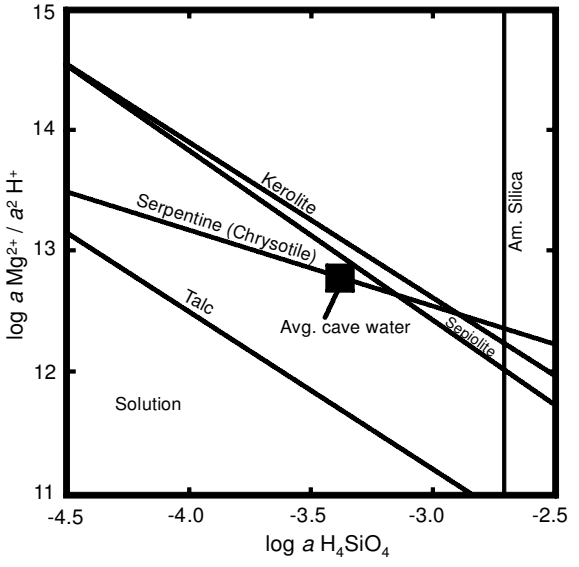

Figure 10. Mineral stabilities of hydrous Mg silicates at 25°C and 1 bar based on thermodynamic data. Modified after Stoessell (1988). Average cave water composition: Mg = 9.5 ppm; Si = 21 ppm; pH = 7.95 (from Léveillé, 2000).

https://doi.org/10.1346/000986002320514235 Published online by Cambridge University Press

difference in their solubilities (Figure 10) is so small that reaction kinetics are probably more important in determining which phase is formed (Stoessell, 1988).

Kerolite is typically interpreted as being a low-temperature weathering product of mafic and ultramafic rocks, and it commonly forms in lacustrine or playa sediments. It can form as an alteration product after sepiolite, Mg-smectite, or more rarely pectolite, or as a direct precipitate (*e.g.* Brindley *et al.*, 1977; Hay *et al.*, 1995; Elton *et al.*, 1997; Pozo and Casas, 1999). Field evidence and kerolite's colloform texture also suggest that it can form from a colloidal suspension or Si-Mg-gel phase (Brindley *et al.*, 1977; Pozo and Casas, 1999).

Experimental evidence suggests that the minimum pH for Mg silicate formation is ~7.80 at ~20°C; sepiolite precipitates at pH ~7.8 to 8.5, trioctahedral Mg-smectite at slightly higher pH, and talc with smectite at pH >9 (Siffert and Wey, 1962). Based on equilibrium-dissolution experiments, a similar pH dependence for kerolite and sepiolite was reported by Stoessell and Hay (1978). Kerolite-like material is believed to have formed directly from groundwaters of pH ~7.9–8.3 at Amboseli (Stoessell and Hay, 1978). Caillère *et al.* (1963) synthesized a poorly-ordered talc-like material from Mg-Si-gels at a pH of 8.0 to 8.9.

Sakamoto *et al.* (1981) produced a 'hydrated talc' (*i.e.* low-crystallinity, hydrated Mg-clay, d_{001} >0.95 nm) with small amounts of serpentine in hydrothermal silicate alteration experiments where $MgCl_2$ was added to solutions to form a MgO-SiO_2 gel. They concluded that Mg ions and Si-O tetrahedra from the silicates form an amorphous MgO-SiO_2 gel, after which the minerals crystallize from the gel with increasing temperature or time. Studies at lower temperatures have also shown the formation of kerolite and kerolite-like minerals from Mg-Si-gels (*cf.* Speakman and Majumdar, 1971; Decarreau *et al.*, 1989).

Origin of the Kauai kerolite and associated minerals

In the Kauai caves, a highly hydrated Mg-Si gel develops on the interior surfaces. This development is probably facilitated by mat-forming bacteria and their abundant extracellular polymers, which decrease diffusion within the mats and concentrate ions from solution (*e.g.* Sánchez-Navas *et al.*, 1998), thus promoting the development of a gel, from which poorly-ordered kerolite is precipitated with time and upon dehydration. The desiccation cracks observed in the kerolite are consistent with this origin. Precipitation of euhedral carbonate crystals within the massive kerolite was also cited as evidence for kerolite formation by dehydration of a gel (Léveillé *et al.*, 2000a). The importance of the microbial mats to kerolite formation is indicated by the general lack of kerolite within basalt vesicles near the rock surface or in thin magnesite-rich evaporative coatings, compared to its abundance in the poorly mineralized microbial mats and lithified microbial deposits (Léveillé *et al.*, 2000a,b).

The abundant EPS may also serve as direct nucleation sites for direct kerolite crystallization by binding and concentrating ions (*e.g.* Mg^{2+}, silica). The presence of a precursor or other substrate can help to overcome kinetic dehydration or nucleation barriers to kerolite formation (Jones, 1986; Hay *et al.*, 1995). Direct nucleation of clay minerals on EPS was observed by Barker and Banfield (1998). Binding of Si^{4+} is probably not important because in these cave waters (pH ≈8; Léveillé, 2000), most Si is in the form H_4SiO_4 (Langmuir, 1997). Bacteria have also been implicated in silicate mineral formation by binding anions (*e.g.* $H_3SiO_4^-$) to positively-charged sites on the cell surface and presumably EPS as well, and by ion-bridging (Urrutia and Beveridge, 1994; Konhauser and Urrutia, 1999). Although there is no direct evidence for such behavior in the present samples, Si is commonly concentrated with Mg in the EPS, as revealed by TEM-EDS analysis (Figure 7).

Other microbial processes within the mats may also lead to changes in solution properties and composition within micro-environments (Léveillé, 2000; Léveillé *et al.*, 2000b). Thus, the composition of the precipitating solution may be more favorable for kerolite formation within parts of the mats than outside of them. For instance, an increase in pH caused by photosynthetic cyanobacteria will tend to favor kerolite formation at the Mg and Si concentrations found in the Kauai caves (Figure 10).

The lack of sepiolite or stevensite in the present deposits suggests that solution chemistry varies and (or) the kinetics for metastable kerolite formation may be more favorable, as the cave waters appear to be close to saturation with respect to all these Mg silicates (Léveillé, 2000). Sepiolite is known to have formed in granitic caves by evaporative concentration of waters after calcite precipitation, but this was in very low-Mg waters (<2 ppm) with relatively high Si concentrations (Finlayson and Webb, 1988). In the Kauai caves, and especially within microbial mats, the $a SiO_2/a Mg^{2+}$ is probably sufficiently low, and the pH sufficiently high to prevent sepiolite formation, and instead, to favor kerolite (Figure 10). The initial presence of Ca^{2+} in solution (and within the microbial mats) may also have favored kerolite formation, as suggested by the experimental results of Sakamoto *et al.* (1981). Minor evaporative concentration of the cave solutions could also be sufficient to lead the reaction path rapidly through the sepiolite stability field into the kerolite stability field as Mg concentrations increase (Léveillé, 2000; Figure 10). However, evaporation is probably not the major mechanism for kerolite formation in the caves, as it has formed throughout the paragenetic sequence, except as part of the late-stage evaporative coatings rich in magnesite and gypsum (Léveillé *et al.*, 2000a).

Initial formation of an amorphous 1:1 serpentine-like precursor phase would slightly reduce the Mg/Si ratio

enabling the 2:1 kerolite to subsequently precipitate without significant evaporation (*cf.* Sakamoto *et al.*, 1981). Santiago Buey *et al.* (2000) reached a similar conclusion for poorly-crystalline Mg silicates. They suggested that the precursor-clay material acts as incipient nucleation sites for fine-grained Mg-clay, in that case stevensite. Thus, the putative serpentine in the present deposits may simply be an early-stage amorphous precursor, which is later transformed into a slightly more ordered kerolite.

Serpentine may also originate as a direct alteration product of the basalt, possibly within the soil weathering profile, and be transported subsequently to the cave below. However, the serpentine present in soils and in partially weathered basalt on Kauai is relatively well crystallized and easily recognized by XRD (Patterson, 1971). The small amount of kaolinite in the cave deposits may also have been transported from the soils, as it too is a common Kauai soil constituent (Patterson, 1971).

Bacteria and Mg-clay formation

Despite the increasing awareness of the role of bacteria and microbial mats in neoformation of clay minerals, nearly all such work has focused on Fe-Al clays (Tazaki, 1997; Konhauser and Urrutia, 1999). The role of bacteria in Mg-clay formation has received very little study, probably because evaporation of solutions or alteration of mineral precursors are typically cited as the modes of formation for such minerals. Renaut and Jones (1997) have described thin (<20 μm) reticulate gelatinous coatings with a high Si and Mg content covering surfaces of aragonite and calcite crystals in hot spring travertines. These authors suggested that some of the coatings originated as bacterial extracellular polymeric substances, while others are siliceous gels precipitated directly from solution. However, no crystalline Mg silicates were identified by Renaut and Jones (1997). The Kauai cave deposits may provide the first evidence for a bacterial influence on neoformation of Mg-clay minerals.

CONCLUSIONS

An abundant 1.0 nm, non-expanding, 2:1 Mg-clay mineral present within carbonate-rich speleothems and microbial mats in basaltic sea caves on Kauai, Hawaii, was identified as kerolite. X-ray diffraction analyses and electron microscope observations indicate that this kerolite is extremely poorly ordered; it is also the dominant clay mineral in these deposits. Chemical and thermal analyses suggest that the kerolite may be mixed with smaller amounts of another poorly-ordered, Mg-rich silicate, most likely an amorphous kerolite precursor or a serpentine-like phase, although the latter's presence is inferred, not proven. Structural formula calculations for the kerolite result in an excess of Mg and a deficiency of Si, probably because of the presence of serpentine and (or) the extreme disorder of the kerolite. Kerolite formation in the Kauai caves is partly mediated by the presence of microbial mats and microbial processes within the mats; minor evaporation may also contribute to its formation. This microbial mediation may explain the poor ordering of the kerolite crystals.

ACKNOWLEDGMENTS

We thank Yves Thibault for assistance with the electron probe analyses, and Ron Smith (UWO) and Bob Harris (Guelph) for guidance with the TEM. Paul Middlestead, Kim Law and Li Huang assisted with the clay separations, X-ray diffraction and thermal analysis. This research was supported by the Natural Sciences and Engineering Research Council of Canada (NSERC) grants to WSF and FJL, and a postgraduate scholarship to RJL.

REFERENCES

Barker, W.W. and Banfield, J.F. (1998) Zones of chemical and physical interaction at interfaces between microbial communities and minerals: A model. *Geomicrobiology Journal*, **15,** 223–244.

Bish, D.L. and Brindley, G.W. (1978) Deweylites, mixtures of poorly crystalline hydrous serpentine and talc-like minerals. *Mineralogical Magazine*, **42,** 75–79.

Brindley, G.W. and Brown, G. (editors) (1980) *Crystal Structures of Clay Minerals and their X-ray Identification.* Monograph **5**, Mineralogical Society, London, 495 pp.

Brindley, G.W., Bish, D.L. and Wan, H.M. (1977) The nature of kerolite, its relation to talc and stevensite. *Mineralogical Magazine*, **41,** 443–452.

Caillère, S., Henin, S. and Esteoule, J. (1963) Nouvelles études sur la synthèse des minéraux argileux à partir de gels. *Clay Minerals Bulletin*, **5,** 272–278.

Decarreau, A., Mondesir, H. and Besson, G. (1989) Synthèse et stabilité des stévensites, kérolites et talcs, magnésiens et nickelifères, entre 80 et 240°C. *Comptes Rendus de l'Académie des Sciences Paris*, **308 (II),** 301–306.

Elton, N.J., Hooper, J.J. and Holyer, V.A.D. (1997) An occurrence of stevensite and kerolite in the Devonian Crousa gabbro at Dean Quarry, The Lizard, Cornwall, England. *Clay Minerals*, **32,** 241–252.

Finlayson, B.L. and Webb, J.A. (1988) Evolution of ground water in Californian granites: Evidence from speleothems. *GSA Bulletin*, **100,** 639–645.

Gíslason, S.R., Veblen, D.R. and Livi, K.J.T. (1993) Experimental meteoric water-basalt interactions: Characterization and interpretation of alteration products. *Geochimica et Cosmochimica Acta*, **57,** 1459–1471.

Hay, R.L., Pexton, R.E., Teague, T.T. and Kyser, T.K. (1986) Spring-related carbonate rocks, Mg clays and associated minerals in Pliocene deposits of the Amargosa Desert, Nevada and California. *GSA Bulletin*, **97,** 1488–1503.

Hay, R.L., Hughes, R.E., Kyser, T.K., Glass, H.D. and Liu, J. (1995) Magnesium-rich clays of the Meerschaum mines in the Amboseli Basin, Tanzania and Kenya. *Clays and Clay Minerals*, **43,** 455–466.

Hill, C. and Forti, P. (1997) *Cave Minerals of the World.* National Speleological Society, Huntsville, Alabama, 238 pp.

Jones, B.F. (1986) *Clay mineral diagenesis in lacustrine sediments.* US Geological Survey Bulletin, #1578, Washington D.C., 292–300.

Kashima, N. (1993) Speleominerals of Japanese Islands. *Proceedings of the International Congress on Speleology*, **11,** 75–76.

Konhauser, K.O. and Urrutia, M.M. (1999) Bacterial clay authigenesis: a common geochemical process. *Chemical Geology*, **161,** 399–413.

Langmuir, D. (1997) *Aqueous Environmental Geochemistry*. Prentice Hall, Upper Saddle River, N.J., 600 pp.

Léveillé, R.J. (2000) Biogeochemistry of carbonate-silicate deposits associated with microbial mats in basaltic caves, Kauai, Hawaii. Ph.D. thesis, The University of Western Ontario, London, Canada, 178 pp.

Léveillé, R.J., Fyfe, W.S. and Longstaffe, F.J. (2000a) Unusual secondary Ca-Mg-carbonate-kerolite deposits in basaltic caves, Kauai, Hawaii. *Journal of Geology*, **108,** 613–621.

Léveillé, R.J., Fyfe, W.S. and Longstaffe, F.J. (2000b) Geomicrobiology of carbonate-silicate microbialites from Hawaiian basaltic sea caves. *Chemical Geology*, **169,** 341–357.

Mackenzie, R.C. (1970) *Differential Thermal Analysis*. Academic Press, London, 775 pp.

Maksimović, Z. (1966) β-kerolite-pimelite series from Goleš mountain, Yugoslavia. *Proceedings of the International Clay Conference, Jerusalem*, **1,** 97–105.

Martin de Vidales, J.L., Pozo, M., Alia, J.M., Garcia-Navarro, F. and Rull, F. (1991) Kerolite-stevensite mixed-layers from the Madrid Basin, Central Spain. *Clay Minerals*, **26,** 329–342.

Morandi, N. and Poppi, L. (1974) Studio mineralogico della 'Deweylite' e della 'Gymnite' di Mezzavalle (Predazzo). *Mineralogica et Petrographica Acta*, **20,** 49–61.

Ostrom, M.E. (1961) Separation of clay minerals from carbonate rocks by using acid. *Journal of Sedimentary Petrology*, **31,** 123–129.

Patterson, S.H. (1971) *Investigations of ferruginous bauxite and other mineral resources on Kauai and a reconnaissance of ferruginous bauxite deposits on Maui, Hawaii.* US Geological Survey Professional Paper #656. Washington, D.C.

Polyak, V.J. and Güven, N. (2000) Authigenesis of trioctahedral smectite in magnesium-rich carbonate speleothems in Carlsbad Cavern and other caves of the Guadalupe Mountains, New Mexico. *Clays and Clay Minerals*, **48,** 317–321.

Pozo, M. and Casas, J. (1999) Origin of kerolite and associated Mg clays in palustrine-lacustrine environments. The Esquivias deposit (Neogen Madrid Basin, Spain). *Clay Minerals*, **34,** 395–418.

Renaut, R.W. and Jones, B. (1997) Controls on aragonite and calcite precipitation in hot spring travertines at Chemurkeu, Lake Bogoria, Kenya. *Canadian Journal of Earth Sciences*, **34,** 801–818.

Sakamoto, T., Koshimizu, H., Shinoda, S. and Otsuka, R. (1981) Hydrothermal transformations of some minerals into stevensite. *Proceedings of the 7th International Clay Conference, Bologna and Pavia*, 537–546.

Sánchez-Navas, A., Martín-Algarra, A. and Nieto, F. (1998) Bacterially-mediated authigenesis of clays in phosphate stromatolites. *Sedimentology*, **45,** 519–533.

Santiago Buey, C., Suárez Barrios, M., García Romero, E. and Doval Montoya, M. (2000) Mg-rich smectite 'precursor' phase in the Tagus Basin, Spain. *Clays and Clay Minerals*, **48,** 366–373.

Sarkar, P.K., Friedman, G.M. and Karmalkar, N.R. (1998) Speleothem deposits developed in caves and tunnels of Deccan-Trap basalts, Maharashtra, India. *Carbonates and Evaporites*, **13,** 132–135.

Siffert, B. and Wey, R. (1962) Synthèse d'une sépiolite à température ordinaire. *Comptes Rendus Hebdomadaires des Séances de l'Académie des Sciences*, **254,** 1460–1462.

Speakman, K. and Majumdar, A.J. (1971) Synthetic 'deweylite'. *Mineralogical Magazine*, **38,** 225–234.

Stoessell, R.K. (1988) 25°C and 1 atm dissolution experiments of sepiolite and kerolite. *Geochimica et Cosmochimica Acta*, **52,** 365–374.

Stoessell, R.K. and Hay, R.L. (1978) The geochemical origin of sepiolite and kerolite at Amboseli, Kenya. *Contributions to Mineralogy and Petrology*, **65,** 255–267.

Tazaki, K. (1997) Biomineralization of layer silicates and hydrated Fe/Mn oxides in microbial mats: An electron microscopical study. *Clays and Clay Minerals,* **45,** 203–212.

Urrutia, M.M. and Beveridge, T.J. (1994) Formation of fine-grained metal and silicate precipitates on a bacterial surface (*Bacillus subtilis*). *Chemical Geology*, **116,** 261–280.

Waters, A.C., Donnelly-Nolan, J.M. and Rogers, B.W. (1990) *Selected caves and lava-tube systems in and near Lava Beds National Monument, California*. US Geological Survey Bulletin #1673. Washington D.C.

White, W.B. (1976) Cave minerals and speleothems. Pp. 267–327 in: *The Science of Speleology* (T.D. Ford and C.H.D. Cullingford, editors). Academic Press, London.

(*Received 11 June 2001; revised 15 February 2002; Ms. 557*)